

# Theory of Pressure Dependence of Superconductivity in Bilayer Nickelate $\text{La}_3\text{Ni}_2\text{O}_7$

Kai-Yue Jiang<sup>1,\*</sup>, Yu-Han Cao<sup>2,\*</sup>, Qing-Geng Yang<sup>2,\*</sup>, Hong-Yan Lu<sup>1,†</sup> and Qiang-Hua Wang<sup>2,3,‡</sup>

<sup>1</sup>*School of Physics and Physical Engineering, Qufu Normal University, Qufu 273165, China*

<sup>2</sup>*National Laboratory of Solid State Microstructures & School of Physics, Nanjing University, Nanjing 210093, China*

<sup>3</sup>*Collaborative Innovation Center of Advanced Microstructures, Nanjing University, Nanjing 210093, China*

The recent experiment shows the superconducting transition temperature in the Ruddlesden-Popper bilayer  $\text{La}_3\text{Ni}_2\text{O}_7$  decreases monotonically with increasing pressure above 14 GPa. In order to unravel the underlying mechanism for this unusual dependence, we performed theoretical investigations by combining the density functional theory (DFT) and the unbiased functional renormalization group (FRG). Our DFT calculations show that the Fermi pockets are essentially unchanged with increasing pressure (above 14 GPa), but the bandwidth is enlarged, and particularly the interlayer hopping integral between the nickel  $3d_{3z^2-r^2}$  orbitals is enhanced. From the DFT band structure, we construct the bilayer tight-binding model in terms of the nickel  $3d_{3z^2-r^2}$  and  $3d_{x^2-y^2}$  orbitals. On this basis, we investigate the superconductivity induced by correlation effects by FRG calculations. We find consistently  $s_{\pm}$ -wave pairing triggered by spin fluctuations, but the latter are weakened by pressure and lead to a decreasing transition temperature versus pressure, in qualitative agreement with the experiment. We emphasize that the itinerancy of the  $d$ -orbitals is important and captured naturally in our FRG calculations, and we argue that the unusual pressure dependence would be unnatural, if not impossible, in the otherwise local-moment picture of the nickel  $d$ -orbitals. This sheds lights on the pertinent microscopic description of, and more importantly the mechanism of superconductivity in  $\text{La}_3\text{Ni}_2\text{O}_7$ .

*Introduction.* Following the discovery of cuprate and iron-based high-temperature superconductors, the signature of superconductivity in the bilayer Ruddlesden-Popper (RP)  $\text{La}_3\text{Ni}_2\text{O}_7$  (La327), with a critical temperature  $T_c$  near 80 K above 14 GPa [1], has been attracting widespread research interest, both experimentally [2–22] and theoretically [22–65]. La327 features a  $\text{NiO}_2$  plane, akin to the  $\text{CuO}_2$  plane in cuprates, exhibiting quasi-two-dimensionality. The average valence states of nickel (Ni) atoms in La327 is  $\text{Ni}^{2.5+}$  ( $3d^{7.5}$ ), with the mixed valence states between  $3d^8$  and  $3d^7$ . The  $3d_{3z^2-r^2}$  and  $3d_{x^2-y^2}$  orbitals are approximately half-filled and quarter filled, respectively, and are active near the Fermi level ( $E_F$ ). In view of the three Fermi pockets and the multi-orbital nature, La327 is closer to the situation in iron pnictides. In comparison, in the infinite-layer nickelates, the valence state is  $\text{Ni}/\text{Cu}^{1+}$  ( $3d^9$ ) and is closer to cuprates [66–68]. The theories proposed for La327 so far suggest that the strong vertical interlayer coupling between the Ni  $3d_{3z^2-r^2}$  orbitals is important in driving Cooper pairing, with  $s_{\pm}$ -wave pairing symmetry [24, 26, 27, 34–36, 39, 47–49, 54, 55], or  $d$ -wave pairing symmetry [41–46, 51, 57, 63].

Very recently, a comprehensive high pressure experiment up to 104 GPa is performed for the bilayer RP La327 single crystals [69]. From 0 to 14 GPa, La327 exhibits the  $Amm$  space group and remains weakly insulating. Above 14 GPa, it undergoes a phase transition to the  $I4/mmm$  structure and enters the superconducting state. The transition temperature decreases monotonically from 83 K at 18 GPa, where the superconductivity just emerges with pressure, and drops to below 40 K for pressures above 90 GPa, forming a right-triangle shape in the temperature-pressure phase diagram. We argue that

this pressure dependence is unusual. First, we can rule out the role of electron-phonon coupling, since the transition temperature is well above the McMillan limit ( $\sim 40$  K) [70]. On the other hand, the pressure dependence should be inconsistent with the local-moment picture of the electrons, such as the multi-orbital  $t$ - $J$  model. In such a picture, a rough estimate of the transition temperature is  $T_c \sim J \exp[-\frac{1}{N_F J}]$ , where  $J$  is the effective spin-exchange and  $N_F$  is the density of states (DOS) at the  $E_F$ . We observe that  $J \propto t^2$  and  $N_F \propto 1/t$ , where  $t$  is a representative hopping integral. Since  $t$  should increase under hydro-static pressure, we see that both  $J$  and  $N_F J$  would increase with pressure, yielding an increasing  $T_c$ , which is apparently at odd with the experiment [69]. It is therefore important to ask whether the unusual pressure dependence of  $T_c$  in La327 could be understood in the itinerant picture. In turn, the experimental pressure dependence can be used to judge the relevance of the itinerant picture and subsequently unravel the mechanism of superconductivity.

In this Letter, we systematically study the electronic structures of La327 in the experimental pressure regime by density functional theory, construct the bilayer two-orbital tight-binding model in terms of the  $3d_{3z^2-r^2}$  and  $3d_{x^2-y^2}$  orbitals of Ni, and then analyze the correlation effects and superconductivity by the unbiased singular-mode functional renormalization group (SM-FRG). We demonstrate that the pairing symmetry is consistently  $s_{\pm}$ -wave, and the pairing is triggered by spin fluctuations, which are weakened by increasing pressure, leading to monotonic decrease of the transition temperature, in qualitative agreement with the experiment. The results support the itinerant picture of the pairing in the bilayer La327 under high pressures.

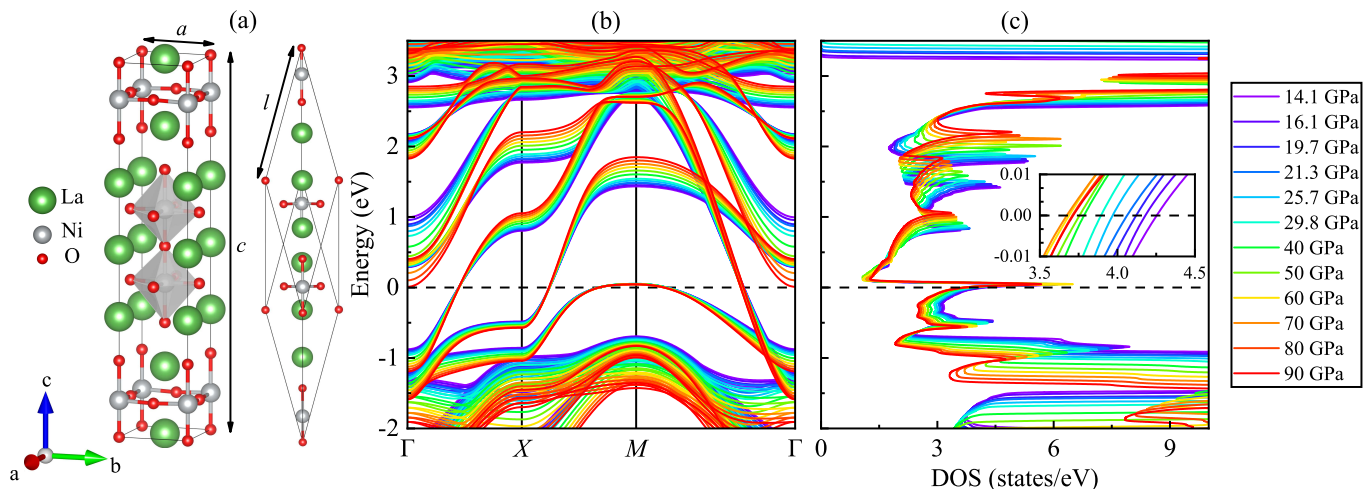


FIG. 1. (a) Conventional cell and primitive cell for La327 under high pressure. (b) Band structure and (c) DOS under different pressures. The subfigure shows the DOS near the  $E_F$ .

*Electronic model.* The lattice structure of La327 under high-pressure with  $I4/mmm$  space group is shown in Fig. 1(a). The electronic structures are performed by DFT calculations as implemented in Vienna *ab initio* simulation package (VASP) [71]. The projector augmented-wave (PAW) [72] method and the generalized gradient approximation (GGA) of Perdew-Burke-Ernzerhof (PBE) [73] exchange-correlation functional are adopted. The cutoff energy of plane-wave is set as 500 eV. The  $\Gamma$ -centered  $12 \times 12 \times 12$  and  $36 \times 36 \times 36$   $k$ -point grids for the self-consistent and DOS calculations are used, respectively. Based on the experimental lattice parameters listed in Table I, fully optimization is carried out on the lattice parameters and atomic positions. The optimized lattice parameters are also shown in Table I. By comparison, the difference between experimental and theoretical lattice values of La327 is less than (about) 1% for  $a$  ( $c$ ,  $l$ ), which is within a reasonable error. Besides, with the increase of pressure, the lattice parameters decrease monotonically. Additionally, we compare the electronic structures calculated using both experimental and theoretical lattice parameters shown in Fig. S1 [74] (which also contains Refs. [75–81]) and find no significant difference, which confirms the reliability of theoretical calculation. Due to the fact that the lattice parameter are only measured up to 29.8 GPa experimentally, while we need to study the electronic structure and superconductivity up to 90 GPa, our calculations are based on the theoretically calculated lattice parameters in order to maintain consistency in our research. The band structures and DOS under different pressures are shown in Figs. 1(b) and 1(c). As the pressure increases, it is found that the Fermi points at  $E_F$  remain almost unchanged, while the dispersion far from the  $E_F$  are significantly separated, enlarging the band width. Moreover, with increasing pressure, the DOS at the  $E_F$  first decreases and then increases slightly

TABLE I. The lattice parameters ( $\text{\AA}$ ) under different pressures (GPa) from experiment (exp.) and DFT calculation (cal.), where  $a$  and  $c$  ( $l$ ) represent the conventional cell (primitive cell) lattice parameters.

Pressure	$a_{\text{exp.}}$	$c_{\text{exp.}}$	$l_{\text{exp.}}$	$a_{\text{cal.}}$	$c_{\text{cal.}}$	$l_{\text{cal.}}$
14.1	3.756	20.020	10.356	3.754	19.788	10.244
16.1	3.747	19.967	10.329	3.743	19.724	10.211
19.7	3.732	19.833	10.262	3.725	19.628	10.161
21.3	3.726	19.746	10.218	3.717	19.583	10.138
25.7	3.710	19.648	10.168	3.698	19.471	10.080
29.8	3.686	19.591	10.136	3.679	19.375	10.031
40.0	-	-	-	3.640	19.159	9.919
50.0	-	-	-	3.605	18.976	9.825
60.0	-	-	-	3.574	18.809	9.738
70.0	-	-	-	3.546	18.663	9.662
80.0	-	-	-	3.520	18.527	9.592
90.0	-	-	-	3.450	18.402	9.527

after 70 GPa, as shown in the subfigure in Fig. 1(c). Combining the orbital-projected band structure and partial DOS as shown in Figs. S2(a) and S2(b) at 14.1 GPa [74], it is evident that the states near the  $E_F$  are dominated by nickel  $3d_{3z^2-r^2}$  and  $3d_{x^2-y^2}$  orbitals, which is consistent with previous studies on La327 [1, 23, 25–27, 55]. In Fig. S2(c) [74], the three-dimensional Fermi surface is displayed, which exhibits two-dimensional-like feature.

Subsequently, the maximally localized Wannier functions [82, 83] of La327 with  $3d_{3z^2-r^2}$  and  $3d_{x^2-y^2}$  orbitals on each Ni atom are extracted by the Wannier90 code [84]

TABLE II. On-site energies  $\varepsilon_a$  and hopping integrals  $t_\delta^{ab}$  of the bilayer two-orbital tight-binding model for La327 under different pressures. Here,  $x/z$  denotes the  $3d_{x^2-y^2}/3d_{3z^2-r^2}$  orbital. Note that the vertical interlayer distance is assigned as  $\frac{1}{2}$ . The unit of pressure is GPa, and the unit of  $\varepsilon_a$  and  $t_\delta^{ab}$  are eV.

Pressure	$\varepsilon_x$	$\varepsilon_z$	$t_{(100)}^{xx}$	$t_{(100)}^{zz}$	$t_{(100)}^{xz}$	$t_{(00\frac{1}{2})}^{xx}$	$t_{(00\frac{1}{2})}^{zz}$	$t_{(110)}^{xx}$	$t_{(110)}^{zz}$	$t_{(10\frac{1}{2})}^{xz}$
14.1	0.728	0.402	-0.470	-0.118	0.235	0.008	-0.623	0.071	-0.018	-0.036
16.1	0.737	0.407	-0.476	-0.119	0.238	0.009	-0.629	0.071	-0.018	-0.037
19.7	0.747	0.411	-0.483	-0.121	0.242	0.009	-0.637	0.071	-0.018	-0.037
21.3	0.749	0.412	-0.486	-0.123	0.243	0.008	-0.640	0.071	-0.018	-0.037
25.7	0.761	0.416	-0.495	-0.125	0.247	0.009	-0.647	0.072	-0.018	-0.037
29.8	0.769	0.417	-0.501	-0.126	0.249	0.010	-0.651	0.072	-0.018	-0.036
40.0	0.803	0.426	-0.521	-0.134	0.259	0.009	-0.674	0.071	-0.015	-0.040
50.0	0.833	0.437	-0.535	-0.139	0.269	0.010	-0.698	0.073	-0.016	-0.042
60.0	0.847	0.435	-0.552	-0.145	0.273	0.011	-0.703	0.075	-0.016	-0.040
70.0	0.871	0.447	-0.566	-0.149	0.283	0.010	-0.723	0.073	-0.017	-0.041
80.0	0.896	0.453	-0.580	-0.153	0.287	0.009	-0.738	0.072	-0.015	-0.045
90.0	0.918	0.461	-0.593	-0.155	0.293	0.008	-0.753	0.071	-0.016	-0.046

to construct a bilayer two-orbital tight-binding model

$$H_0 = \sum_{i\delta, ab, \sigma} t_\delta^{ab} c_{ia\sigma}^\dagger c_{i+\delta b\sigma} + \sum_{ia\sigma} \varepsilon_a c_{ia\sigma}^\dagger c_{ia\sigma}, \quad (1)$$

where  $t_\delta^{ab}$  is the hopping matrix element between the  $a$  orbital on site  $i$  and the  $b$  orbital on site  $i + \delta$ ,  $\sigma$  represents spin, and  $\varepsilon_a$  is the on-site energy of the  $a$ -orbital. For simplicity,  $x$  and  $z$  represent the  $3d_{x^2-y^2}$  and  $3d_{3z^2-r^2}$  orbitals in the following, respectively. The good overlapping between DFT and Wannier band structures is also displayed in Fig. S3 [74], indicating the high quality of Wannier functions. The on-site energy and hopping parameters are listed in Table II. The vertical interlayer hopping between the  $z$ -orbitals  $t_{(00\frac{1}{2})}^{zz}$  is found to be the strongest, consistent with previous studies in La327 [23, 26, 27].

In Fig. 2(a), we plot the band structures of the tight-binding parameters at each pressure listed in Table II. They reproduce nicely the DFT results in Fig. 1(b). The splitting of the band dispersion can be understood as follows. The Hamiltonian can be expressed as a block-diagonal form in the bonding and anti-bonding orbital basis, which hence, gives a perfect diagonal matrix with decoupled  $x$  and  $z$  orbital bands along the  $M$ - $\Gamma$  line due to the loss of the inter-orbital hopping [23]. Specifically at high symmetry points  $M$  and  $\Gamma$ , we have the  $x/z$  orbital bonding (+) and anti-bonding (-) energies  $E_{M,\pm}^{x/z} = -4t_{100}^{xx/zz} + 4t_{110}^{x/z} + \varepsilon_{x/z} \pm t_{00\frac{1}{2}}^{x/z}$  and  $E_{\Gamma,\pm}^{x/z} = 4t_{100}^{xx/zz} + 4t_{110}^{x/z} + \varepsilon_{x/z} \pm t_{00\frac{1}{2}}^{x/z}$ . According to Table II and Fig. S5 [74], these energies monotonically

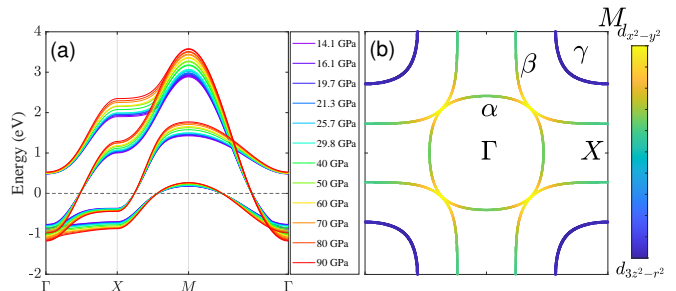


FIG. 2. (a) Tight-binding band structures of La327 at pressures listed in Table II. (b) Fermi surfaces obtained from the parameters shown at the pressure 14.1 GPa. The orbital weights of  $d_{x^2-y^2}$  and  $d_{3z^2-r^2}$  are represented by colors directly.

change with the pressure, which leads to the dispersion splitting. On the other hand, the barely changed Fermi points in the dispersion implies the Fermi pockets are not changed under pressures. This is indeed the case from our explicit calculation of the Fermi pockets and the orbital contents. This can be explained by the concurrent change of the tight-binding parameters under pressure, see Fig. S6 [74]. One typical result at pressure 14.1 GPa is shown in Fig. 2(b). Similarly to the previous theoretical works [23, 24], there are three Fermi pockets  $\alpha$ ,  $\beta$  and  $\gamma$ . The  $\alpha$  and  $\beta$  pockets have mixed orbital weights (except in the diagonal direction), while the  $\gamma$  pocket is dominated by the  $d_{3z^2-r^2}$  orbital.

*FRG analysis.* The well-constructed tight-binding models discussed above enables us to study the super-

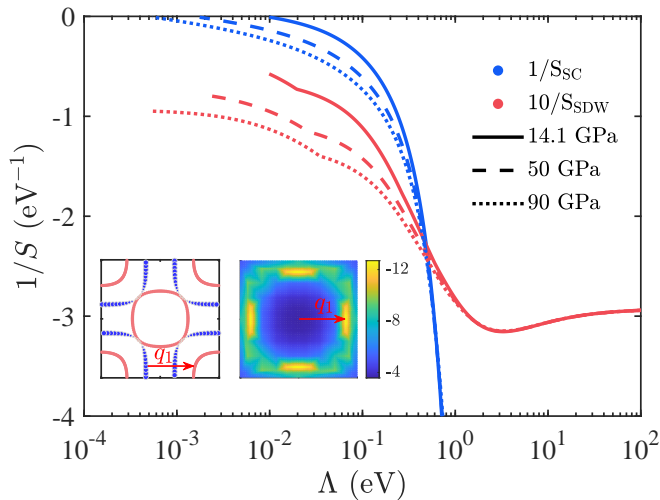


FIG. 3. FRG flows of  $S^{-1}$  versus  $\Lambda$  in the SC and SDW channels of La327, respectively, at pressures 14.1, 50, and 90 GPa. The left subfigure present the gap function on the Fermi surfaces. The right subfigure present the leading negative  $S(\mathbf{q})$  in the SDW channel. Both subfigures are the results at pressure 50 GPa.

conductivity driven by correlation effects in La327 system under pressure. In this Letter, we use SM-FRG to calculate the one-particle-irreducible four-point vertex  $\Gamma_{\Lambda}$  iteratively against a running infrared cutoff energy scale  $\Lambda$ . The same vertex  $\Gamma_{\Lambda}$  is re-expressed as scattering matrices between fermion bilinears in the superconducting (SC), spin-density-wave (SDW) and charge-density-wave (CDW) channels. We monitor the negative leading eigenvalue  $S$  of these scattering matrices during the FRG flow. The first divergence of the  $S$  (among the three channels) at the scale  $\Lambda_c$  signals an emerging order described by the scattering channel, the scattering momentum, and the eigen scattering mode. In addition to the fact that the SM-FRG treats all possible orderings on equal footing, it has the further advantage to obtain directly the transition temperature  $T_c \sim \Lambda_c$ . More technical details can be found in Refs. [24, 78, 80, 85, 86] and the Supplemental Material [74]. In the following, we first show three typical FRG results at different cases, followed by the discussion on the systematic pressure dependence of  $T_c$ .

In Fig. 3, we plot the inverse of the values  $S$  versus  $\Lambda$  in the SC and SDW channels, respectively, at pressures 14.1, 50, and 90 GPa. The CDW channel is much weaker and omitted for clarity. We choose the intra-orbital Hubbard repulsion  $U = 3$  eV and Hund's coupling  $J_H = 0.4$  eV. The Kanamori relations are also used, so that we have the interorbital repulsion  $U' = U - 2J_H$  and inter-orbital pair-hopping  $J_P = J_H$ . The initial FRG flows at higher energy scales are quite similar for the three different pressures, where the bare interactions dominate and hence the SDW channel is stronger. At

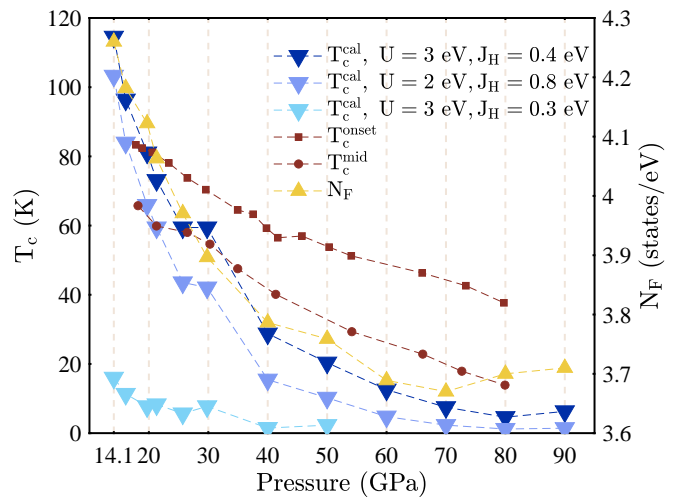


FIG. 4. Phase diagram of superconducting  $T_c$  versus pressure of La327. The  $T_c^{onset}$  and  $T_c^{mid}$  are extracted from the experimental work [69] for comparison.

low energy scales, however, the SDW channel becomes subleading and turns to saturate because of the lack of phase space for low-energy particle-hole excitations. The momentum dependent eigenvalue in the SDW channel is presented in the right inset, showing peaks in the (1,0) and (0,1) directions. At intermediate energy scales where the SDW channel grows, the SC channel begins to be induced through channel overlap. The latter then eventually diverges by Cooper mechanism. This is a typical manifestation of spin fluctuation mediated superconductivity. Similar results are obtained for all cases listed in Table II. From the eigen scattering mode in the SC channel, we obtain the pairing gap function on the Fermi pockets (left inset), showing  $s_{\pm}$ -wave symmetry. Up to  $C_{4v}$  symmetry, there exists a momentum  $\mathbf{q}_1$  that connects two Fermi pockets with opposite pairing signs. This particular momentum is just the peak momentum in the SDW channel (right inset), which reconfirms the connection between pairing and spin fluctuations here.

We see from Fig. 3 that the critical energy scale  $\Lambda_c$  drastically drops as the pressure increases from 14.1 to 50 GPa and 90 GPa, and this can be clearly related to the weakening of spin fluctuations (at the final stage of FRG flow). This implies the high sensitivity of the transition temperature  $T_c \sim \Lambda_c$  on the pressure. We therefore perform systematic SM-FRG calculations for a sequence of pressures listed in Table II to obtain the pressure dependence of the transition temperature  $T_c^{cal}$  shown in Fig. 4 (down triangles). The experimental data of superconducting  $T_c^{onset}$  (filled squares) and  $T_c^{mid}$  (filled circles) [69] are also displayed for comparison. Remarkably, there is a notable consistency between the calculated results and the experimental observations. Moreover, to see the robustness of our SM-FRG results, we have performed systematic calculations by varying  $U$  and  $J_H$ . The re-

sults are qualitatively similar, see Fig. 4, except that the lowest  $J_H$  yields the lowest  $T_c$ , implying the importance of Hund's coupling. We also note that while the normal state DOS (yellow triangles) is higher at 80 GPa than that at 70 GPa, our theoretical  $T_c$  does not follow the trend in DOS, but is in agreement with the experiment. This indicates the necessity of treating the band structure and the correlations systematically, as we do in our FRG calculations.

*Conclusion.* Combing the DFT and SM-FRG calculations, the electronic structures, tight-binding model, pairing mechanism, and pairing symmetry are systematically investigated under different pressures in the superconducting regime of La327. We find the pairing symmetry is consistently  $s_{\pm}$ -wave, triggered by spin fluctuations which become increasingly weakened by pressure and consequently lead to decreasing superconducting transition temperature, in qualitative agreement with the experiment. We argue that the pressure dependence is difficult, if not impossible, to be explained by the local-moment picture of the electrons, while the success in our theory sheds light on the importance of the itineracy of electrons in La327, at least in the superconducting regime.

*Acknowledgments.* We thank Meng Wang for experimental data and discussion. This work is supported by National Natural Science Foundation of China (Grant No. 12074213, No. 12374147, No. 12274205, No. 92365203, No. 11874205, and No. 11574108), National Key R&D Program of China (Grant No. 2022YFA1403201), and Major Basic Program of Natural Science Foundation of Shandong Province (Grant No. ZR2021ZD01).

---

\* K.Y.J, Y.H.C, and Q.G.Y. contributed equally to this work.

† [hylu@qfnu.edu.cn](mailto:hylu@qfnu.edu.cn)

‡ [qhwang@nju.edu.cn](mailto:qhwang@nju.edu.cn)

- [1] H. Sun, M. Huo, X. Hu, J. Li, Z. Liu, Y. Han, L. Tang, Z. Mao, P. Yang, B. Wang, J. Cheng, D.-X. Yao, G.-M. Zhang, and M. Wang, Signatures of superconductivity near 80 K in a nickelate under high pressure, *Nature* **621**, 493 (2023).
- [2] Z. Liu, M. Huo, J. Li, Q. Li, Y. Liu, Y. Dai, X. Zhou, J. Hao, Y. Lu, M. Wang, and H.-H. Wen, Electronic correlations and energy gap in the bilayer nickelate  $\text{La}_3\text{Ni}_2\text{O}_7$  (2023), [arXiv:2307.02950](https://arxiv.org/abs/2307.02950) [cond-mat.supr-con].
- [3] J. Hou, P.-T. Yang, Z.-Y. Liu, J.-Y. Li, P.-F. Shan, L. Ma, G. Wang, N.-N. Wang, H.-Z. Guo, J.-P. Sun, Y. Uwatoko, M. Wang, G.-M. Zhang, B.-S. Wang, and J.-G. Cheng, Emergence of high-temperature superconducting phase in pressurized  $\text{La}_3\text{Ni}_2\text{O}_7$  crystals, *Chin. Phys. Lett.* **40**, 117302 (2023).
- [4] Y. Zhang, D. Su, Y. Huang, Z. Shan, H. Sun, M. Huo, K. Ye, J. Zhang, Z. Yang, Y. Xu, Y. Su, R. Li, M. Smidman, M. Wang, L. Jiao, and H. Yuan, High-temperature superconductivity with zero resistance and strange-metal behaviour in  $\text{La}_3\text{Ni}_2\text{O}_{7-\delta}$ , *Nat. Phys.* **10.1038/s41567-024-02515-y** (2024).
- [5] M. Zhang, C. Pei, Q. Wang, Y. Zhao, C. Li, W. Cao, S. Zhu, J. Wu, and Y. Qi, Effects of pressure and doping on Ruddlesden-Popper phases  $\text{La}_{n+1}\text{Ni}_n\text{O}_{3n+1}$ , *J. Mater. Sci. Technol.* **185**, 147 (2024).
- [6] G. Wang, N. Wang, Y. Wang, L. Shi, X. Shen, J. Hou, H. Ma, P. Yang, Z. Liu, H. Zhang, X. Dong, J. Sun, B. Wang, K. Jiang, J. Hu, Y. Uwatoko, and J. Cheng, Observation of high-temperature superconductivity in the high-pressure tetragonal phase of  $\text{La}_2\text{PrNi}_2\text{O}_{7-\delta}$  (2023), [arXiv:2311.08212](https://arxiv.org/abs/2311.08212) [cond-mat.supr-con].
- [7] L. Wang, Y. Li, S.-Y. Xie, F. Liu, H. Sun, C. Huang, Y. Gao, T. Nakagawa, B. Fu, B. Dong, Z. Cao, R. Yu, S. I. Kawaguchi, H. Kadobayashi, M. Wang, C. Jin, H.-k. Mao, and H. Liu, Structure responsible for the superconducting state in  $\text{La}_3\text{Ni}_2\text{O}_7$  at high-pressure and low-temperature conditions, *J. Am. Chem. Soc.* **146**, 7506 (2024).
- [8] Y. Zhou, J. Guo, S. Cai, H. Sun, P. Wang, J. Zhao, J. Han, X. Chen, Q. Wu, Y. Ding, M. Wang, T. Xiang, H. Kwang Mao, and L. Sun, Investigations of key issues on the reproducibility of high- $T_c$  superconductivity emerging from compressed  $\text{La}_3\text{Ni}_2\text{O}_7$  (2023), [arXiv:2311.12361](https://arxiv.org/abs/2311.12361) [cond-mat.supr-con].
- [9] T. Cui, S. Choi, T. Lin, C. Liu, G. Wang, N. Wang, S. Chen, H. Hong, D. Rong, Q. Wang, Q. Jin, J.-O. Wang, L. Gu, C. Ge, C. Wang, J.-G. Cheng, Q. Zhang, L. Si, K.-j. Jin, and E.-J. Guo, Strain-mediated phase crossover in Ruddlesden-Popper nickelates, *Commun. Mater.* **5**, 32 (2024).
- [10] K. Chen, X. Liu, J. Jiao, M. Zou, C. Jiang, X. Li, Y. Luo, Q. Wu, N. Zhang, Y. Guo, and L. Shu, Evidence of spin density waves in  $\text{La}_3\text{Ni}_2\text{O}_{7-\delta}$ , *Phys. Rev. Lett.* **132**, 256503 (2024).
- [11] X. Chen, J. Zhang, A. S. Thind, S. Sharma, H. LaBollita, G. Peterson, H. Zheng, D. P. Phelan, A. S. Botana, R. F. Klie, and J. F. Mitchell, Polymorphism in the Ruddlesden-Popper nickelate  $\text{La}_3\text{Ni}_2\text{O}_7$ : Discovery of a hidden phase with distinctive layer stacking, *J. Am. Chem. Soc.* **146**, 3640 (2024).
- [12] P. Puphal, P. Reiss, N. Enderlein, Y.-M. Wu, G. Khalullin, V. Sundaramurthy, T. Priessnitz, M. Knauff, L. Richter, M. Isobe, P. A. van Aken, H. Takagi, B. Keimer, Y. E. Suyolcu, B. Wehinger, P. Hansmann, and M. Hepting, Unconventional crystal structure of the high-pressure superconductor  $\text{La}_3\text{Ni}_2\text{O}_7$  (2023), [arXiv:2312.07341](https://arxiv.org/abs/2312.07341) [cond-mat.supr-con].
- [13] H. Wang, L. Chen, A. Rutherford, H. Zhou, and W. Xie, Long-range structural order in a hidden phase of Ruddlesden-Popper bilayer nickelate  $\text{La}_3\text{Ni}_2\text{O}_7$ , *Inorg. Chem.* **63**, 5020 (2024).
- [14] M. Kakoi, T. Oi, Y. Ohshita, M. Yashima, K. Kuroki, T. Kato, H. Takahashi, S. Ishiwata, Y. Adachi, N. Hatada, T. Uda, and H. Mukuda, Multiband metallic ground state in multilayered nickelates  $\text{La}_3\text{Ni}_2\text{O}_7$  and  $\text{La}_4\text{Ni}_3\text{O}_{10}$  probed by  $^{139}\text{La}$ -NMR at ambient pressure, *J. Phys. Soc. Jpn.* **93**, 053702 (2024).
- [15] M. Xu, S. Huyan, H. Wang, S. L. Bud'ko, X. Chen, X. Ke, J. F. Mitchell, P. C. Canfield, J. Li, and W. Xie, Pressure-dependent "insulator-metal-insulator" behavior in Sr-doped  $\text{La}_3\text{Ni}_2\text{O}_7$ , *Adv. Electron. Mater.* **n/a**, 2400078 (2024).

- [16] Z. Dong, M. Huo, J. Li, J. Li, P. Li, H. Sun, L. Gu, Y. Lu, M. Wang, Y. Wang, and Z. Chen, Visualization of oxygen vacancies and self-doped ligand holes in  $\text{La}_3\text{Ni}_2\text{O}_{7-\delta}$ , *Nature* **630**, 847 (2024).
- [17] E. F. Talantsev and V. V. Chistyakov, Debye temperature, electron-phonon coupling constant, and microcrystalline strain in highly-compressed  $\text{La}_3\text{Ni}_2\text{O}_{7-\delta}$  (2024), [arXiv:2401.00804](https://arxiv.org/abs/2401.00804) [cond-mat.supr-con].
- [18] B. Geisler, L. Fanfarillo, J. J. Hamlin, G. R. Stewart, R. G. Hennig, and P. J. Hirschfeld, Optical properties and electronic correlations in  $\text{La}_3\text{Ni}_2\text{O}_{7-\delta}$  bilayer nickelates under high pressure (2024), [arXiv:2401.04258](https://arxiv.org/abs/2401.04258) [cond-mat.supr-con].
- [19] J. Yang, H. Sun, X. Hu, Y. Xie, T. Miao, H. Luo, H. Chen, B. Liang, W. Zhu, G. Qu, C.-Q. Chen, M. Huo, Y. Huang, S. Zhang, F. Zhang, F. Yang, Z. Wang, Q. Peng, H. Mao, G. Liu, Z. Xu, T. Qian, D.-X. Yao, M. Wang, L. Zhao, and X. J. Zhou, Orbital-dependent electron correlation in double-layer nickelate  $\text{La}_3\text{Ni}_2\text{O}_7$ , *Nat. Commun.* **15**, 4373 (2024).
- [20] D. Takegami, K. Fujinuma, R. Nakamura, M. Yoshimura, K.-D. Tsuei, G. Wang, N. N. Wang, J.-G. Cheng, Y. Uwatoko, and T. Mizokawa, Absence of  $\text{Ni}^{2+}/\text{Ni}^{3+}$  charge disproportionation and possible roles of  $02p$  holes in  $\text{La}_3\text{Ni}_2\text{O}_{7-\delta}$  revealed by hard x-ray photoemission spectroscopy, *Phys. Rev. B* **109**, 125119 (2024).
- [21] G. Wang, N. N. Wang, X. L. Shen, J. Hou, L. Ma, L. F. Shi, Z. A. Ren, Y. D. Gu, H. M. Ma, P. T. Yang, Z. Y. Liu, H. Z. Guo, J. P. Sun, G. M. Zhang, S. Calder, J.-Q. Yan, B. S. Wang, Y. Uwatoko, and J.-G. Cheng, Pressure-induced superconductivity in polycrystalline  $\text{La}_3\text{Ni}_2\text{O}_{7-\delta}$ , *Phys. Rev. X* **14**, 011040 (2024).
- [22] M. Wang, H.-H. Wen, T. Wu, D.-X. Yao, and T. Xiang, Normal and superconducting properties of  $\text{La}_3\text{Ni}_2\text{O}_7$ , *Chin. Phys. Lett.* (2024).
- [23] Z. Luo, X. Hu, M. Wang, W. Wú, and D.-X. Yao, Bilayer two-orbital model of  $\text{La}_3\text{Ni}_2\text{O}_7$  under pressure, *Phys. Rev. Lett.* **131**, 126001 (2023).
- [24] Q.-G. Yang, D. Wang, and Q.-H. Wang, Possible  $s_{\pm}$ -wave superconductivity in  $\text{La}_3\text{Ni}_2\text{O}_7$ , *Phys. Rev. B* **108**, L140505 (2023).
- [25] Y. Zhang, L.-F. Lin, A. Moreo, and E. Dagotto, Electronic structure, dimer physics, orbital-selective behavior, and magnetic tendencies in the bilayer nickelate superconductor  $\text{La}_3\text{Ni}_2\text{O}_7$  under pressure, *Phys. Rev. B* **108**, L180510 (2023).
- [26] H. Sakakibara, N. Kitamine, M. Ochi, and K. Kuroki, Possible high  $T_c$  superconductivity in  $\text{La}_3\text{Ni}_2\text{O}_7$  under high pressure through manifestation of a nearly half-filled bilayer Hubbard model, *Phys. Rev. Lett.* **132**, 106002 (2024).
- [27] Y. Gu, C. Le, Z. Yang, X. Wu, and J. Hu, Effective model and pairing tendency in bilayer Ni-based superconductor  $\text{La}_3\text{Ni}_2\text{O}_7$  (2023), [arXiv:2306.07275](https://arxiv.org/abs/2306.07275) [cond-mat.supr-con].
- [28] V. Christiansson, F. Petocchi, and P. Werner, Correlated electronic structure of  $\text{La}_3\text{Ni}_2\text{O}_7$  under pressure, *Phys. Rev. Lett.* **131**, 206501 (2023).
- [29] D. A. Shilenko and I. V. Leonov, Correlated electronic structure, orbital-selective behavior, and magnetic correlations in double-layer  $\text{La}_3\text{Ni}_2\text{O}_7$  under pressure, *Phys. Rev. B* **108**, 125105 (2023).
- [30] Y. Shen, M. Qin, and G.-M. Zhang, Effective bi-layer model Hamiltonian and density-matrix renormalization group study for the high- $T_c$  superconductivity in  $\text{La}_3\text{Ni}_2\text{O}_7$  under high pressure, *Chin. Phys. Lett.* **40**, 127401 (2023).
- [31] W. Wú, Z. Luo, D.-X. Yao, and M. Wang, Superexchange and charge transfer in the nickelate superconductor  $\text{La}_3\text{Ni}_2\text{O}_7$  under pressure, *Sci. China Phys. Mech. Astron.* **67**, 117402 (2024).
- [32] Y. Cao and Y.-f. Yang, Flat bands promoted by Hund's rule coupling in the candidate double-layer high-temperature superconductor  $\text{La}_3\text{Ni}_2\text{O}_7$  under high pressure, *Phys. Rev. B* **109**, L081105 (2024).
- [33] X. Chen, P. Jiang, J. Li, Z. Zhong, and Y. Lu, Critical charge and spin instabilities in superconducting  $\text{La}_3\text{Ni}_2\text{O}_7$  (2023), [arXiv:2307.07154](https://arxiv.org/abs/2307.07154) [cond-mat.supr-con].
- [34] Y.-B. Liu, J.-W. Mei, F. Ye, W.-Q. Chen, and F. Yang,  $s_{\pm}$ -wave pairing and the destructive role of apical-oxygen deficiencies in  $\text{La}_3\text{Ni}_2\text{O}_7$  under pressure, *Phys. Rev. Lett.* **131**, 236002 (2023).
- [35] C. Lu, Z. Pan, F. Yang, and C. Wu, Interlayer-coupling-driven high-temperature superconductivity in  $\text{La}_3\text{Ni}_2\text{O}_7$  under pressure, *Phys. Rev. Lett.* **132**, 146002 (2024).
- [36] Y. Zhang, L.-F. Lin, A. Moreo, T. A. Maier, and E. Dagotto, Structural phase transition,  $s_{\pm}$ -wave pairing, and magnetic stripe order in bilayered superconductor  $\text{La}_3\text{Ni}_2\text{O}_7$  under pressure, *Nat. Commun.* **15**, 2470 (2024).
- [37] Y. Zhang, L.-F. Lin, A. Moreo, and E. Dagotto, Electronic structure, dimer physics, orbital-selective behavior, and magnetic tendencies in the bilayer nickelate superconductor  $\text{La}_3\text{Ni}_2\text{O}_7$  under pressure, *Phys. Rev. B* **108**, L180510 (2023).
- [38] H. Oh and Y.-H. Zhang, Type-II  $t-J$  model and shared superexchange coupling from Hund's rule in superconducting  $\text{La}_3\text{Ni}_2\text{O}_7$ , *Phys. Rev. B* **108**, 174511 (2023).
- [39] X.-Z. Qu, D.-W. Qu, J. Chen, C. Wu, F. Yang, W. Li, and G. Su, Bilayer  $t-J-J_{\perp}$  model and magnetically mediated pairing in the pressurized nickelate  $\text{La}_3\text{Ni}_2\text{O}_7$ , *Phys. Rev. Lett.* **132**, 036502 (2024).
- [40] Y.-f. Yang, G.-M. Zhang, and F.-C. Zhang, Interlayer valence bonds and two-component theory for high- $T_c$  superconductivity of  $\text{La}_3\text{Ni}_2\text{O}_7$  under pressure, *Phys. Rev. B* **108**, L201108 (2023).
- [41] F. Lechermann, J. Gondolf, S. Bötzel, and I. M. Eremin, Electronic correlations and superconducting instability in  $\text{La}_3\text{Ni}_2\text{O}_7$  under high pressure, *Phys. Rev. B* **108**, L201121 (2023).
- [42] Z. Liao, L. Chen, G. Duan, Y. Wang, C. Liu, R. Yu, and Q. Si, Electron correlations and superconductivity in  $\text{La}_3\text{Ni}_2\text{O}_7$  under pressure tuning, *Phys. Rev. B* **108**, 214522 (2023).
- [43] K. Jiang, Z. Wang, and F.-C. Zhang, High-temperature superconductivity in  $\text{La}_3\text{Ni}_2\text{O}_7$ , *Chin. Phys. Lett.* **41**, 017402 (2024).
- [44] H. Liu, C. Xia, S. Zhou, and H. Chen, Role of crystal-field-splitting and long-range-hoppings on superconducting pairing symmetry of  $\text{La}_3\text{Ni}_2\text{O}_7$  (2023), [arXiv:2311.07316](https://arxiv.org/abs/2311.07316) [cond-mat.supr-con].
- [45] G. Heier, K. Park, and S. Y. Savrasov, Competing  $d_{xy}$  and  $s_{\pm}$  pairing symmetries in superconducting  $\text{La}_3\text{Ni}_2\text{O}_7$ : LDA + FLEX calculations, *Phys. Rev. B* **109**, 104508 (2024).
- [46] Z. Luo, B. Lv, M. Wang, W. Wú, and D.-X. Yao, High- $T_c$  superconductivity in  $\text{La}_3\text{Ni}_2\text{O}_7$  based on the bilayer two-orbital  $t-J$  model (2023), [arXiv:2308.16564](https://arxiv.org/abs/2308.16564) [cond-mat.supr-con].

- [47] J. Huang, Z. D. Wang, and T. Zhou, Impurity and vortex states in the bilayer high-temperature superconductor  $\text{La}_3\text{Ni}_2\text{O}_7$ , *Phys. Rev. B* **108**, 174501 (2023).
- [48] Y. Zhang, L.-F. Lin, A. Moreo, T. A. Maier, and E. Dagotto, Trends in electronic structures and  $s_{\pm}$ -wave pairing for the rare-earth series in bilayer nickelate superconductor  $R_3\text{Ni}_2\text{O}_7$ , *Phys. Rev. B* **108**, 165141 (2023).
- [49] Y.-H. Tian, Y. Chen, J.-M. Wang, R.-Q. He, and Z.-Y. Lu, Correlation effects and concomitant two-orbital  $s_{\pm}$ -wave superconductivity in  $\text{La}_3\text{Ni}_2\text{O}_7$  under high pressure, *Phys. Rev. B* **109**, 165154 (2024).
- [50] Q. Qin and Y.-F. Yang, High- $T_c$  superconductivity by mobilizing local spin singlets and possible route to higher  $T_c$  in pressurized  $\text{La}_3\text{Ni}_2\text{O}_7$ , *Phys. Rev. B* **108**, L140504 (2023).
- [51] S. Rye, N. Witt, and T. O. Wehling, Quenched pair breaking by interlayer correlations as a key to superconductivity in  $\text{La}_3\text{Ni}_2\text{O}_7$  (2023), [arXiv:2310.17465](https://arxiv.org/abs/2310.17465) [cond-mat.supr-con].
- [52] Z. Ouyang, J.-M. Wang, J.-X. Wang, R.-Q. He, L. Huang, and Z.-Y. Lu, Hund electronic correlation in  $\text{La}_3\text{Ni}_2\text{O}_7$  under high pressure, *Phys. Rev. B* **109**, 115114 (2024).
- [53] X.-Z. Qu, D.-W. Qu, W. Li, and G. Su, Roles of Hund's rule and hybridization in the two-orbital model for high- $T_c$  superconductivity in the bilayer nickelate (2023), [arXiv:2311.12769](https://arxiv.org/abs/2311.12769) [cond-mat.str-el].
- [54] Y.-Y. Zheng and W. Wú, Superconductivity in the bilayer two-orbital Hubbard model (2023), [arXiv:2312.03605](https://arxiv.org/abs/2312.03605) [cond-mat.str-el].
- [55] Y. Wang, K. Jiang, Z. Wang, F.-C. Zhang, and J. Hu, Electronic structure and superconductivity in bilayer  $\text{La}_3\text{Ni}_2\text{O}_7$  (2024), [arXiv:2401.15097](https://arxiv.org/abs/2401.15097) [cond-mat.supr-con].
- [56] M. Kakoi, T. Kaneko, H. Sakakibara, M. Ochi, and K. Kuroki, Pair correlations of the hybridized orbitals in a ladder model for the bilayer nickelate  $\text{La}_3\text{Ni}_2\text{O}_7$ , *Phys. Rev. B* **109**, L201124 (2024).
- [57] Z. Fan, J.-F. Zhang, B. Zhan, D. Lv, X.-Y. Jiang, B. Normand, and T. Xiang, Superconductivity in nickelate and cuprate superconductors with strong bilayer coupling (2023), [arXiv:2312.17064](https://arxiv.org/abs/2312.17064) [cond-mat.supr-con].
- [58] S. Bötzel, F. Lechermann, J. Gondolf, and I. M. Eremin, Theory of magnetic excitations in the multilayer nickelate superconductor  $\text{La}_3\text{Ni}_2\text{O}_7$ , *Phys. Rev. B* **109**, L180502 (2024).
- [59] J.-R. Xue and F. Wang, Magnetism and superconductivity in the  $t$ - $J$  model of  $\text{La}_3\text{Ni}_2\text{O}_7$  under multiband Gutzwiller approximation, *Chin. Phys. Lett.* **41**, 057403 (2024).
- [60] B. Geisler, J. J. Hamlin, G. R. Stewart, R. G. Hennig, and P. J. Hirschfeld, Structural transitions, octahedral rotations, and electronic properties of  $A_3\text{Ni}_2\text{O}_7$  rare-earth nickelates under high pressure, *npj Quantum Mater.* **9**, 38 (2024).
- [61] L. C. Rhodes and P. Wahl, Structural routes to stabilize superconducting  $\text{La}_3\text{Ni}_2\text{O}_7$  at ambient pressure, *Phys. Rev. Mater.* **8**, 044801 (2024).
- [62] L. Craco and S. Leoni, Strange metal and coherence-incoherence crossover in pressurized  $\text{La}_3\text{Ni}_2\text{O}_7$ , *Phys. Rev. B* **109**, 165116 (2024).
- [63] R. Jiang, J. Hou, Z. Fan, Z.-J. Lang, and W. Ku, Pressure driven fractionalization of ionic spins results in cupratelike high- $T_c$  superconductivity in  $\text{La}_3\text{Ni}_2\text{O}_7$ , *Phys. Rev. Lett.* **132**, 126503 (2024).
- [64] H. Lange, L. Homeier, E. Demler, U. Schollwöck, F. Grusdt, and A. Bohrdt, Feshbach resonance in a strongly repulsive ladder of mixed dimensionality: A possible scenario for bilayer nickelate superconductors, *Phys. Rev. B* **109**, 045127 (2024).
- [65] Z. Huo, Z. Luo, P. Zhang, A. Yang, Z. Liu, X. Tao, Z. Zhang, S. Guo, Q. Jiang, W. Chen, D.-X. Yao, D. Duan, and T. Cui, Modulation of the octahedral structure and potential superconductivity of  $\text{La}_3\text{Ni}_2\text{O}_7$  through strain engineering (2024), [arXiv:2404.11001](https://arxiv.org/abs/2404.11001) [cond-mat.supr-con].
- [66] D. Li, K. Lee, B. Y. Wang, M. Osada, S. Crossley, H. R. Lee, Y. Cui, Y. Hikita, and H. Y. Hwang, Superconductivity in an infinite-layer nickelate, *Nature* **572**, 624 (2019).
- [67] P. W. Anderson, The resonating valence bond state in  $\text{La}_2\text{CuO}_4$  and superconductivity, *Science* **235**, 1196 (1987).
- [68] F. C. Zhang and T. M. Rice, Effective Hamiltonian for the superconducting Cu oxides, *Phys. Rev. B* **37**, 3759 (1988).
- [69] J. Li, P. Ma, H. Zhang, X. Huang, C. Huang, M. Huo, D. Hu, Z. Dong, C. He, J. Liao, X. Chen, T. Xie, H. Sun, and M. Wang, Pressure-driven right-triangle shape superconductivity in bilayer nickelate  $\text{La}_3\text{Ni}_2\text{O}_7$  (2024), [arXiv:2404.11369](https://arxiv.org/abs/2404.11369) [cond-mat.supr-con].
- [70] W. L. McMillan, Transition temperature of strong-coupled superconductors, *Phys. Rev.* **167**, 331 (1968).
- [71] G. Kresse and J. Furthmüller, Efficient iterative schemes for *ab initio* total-energy calculations using a plane-wave basis set, *Phys. Rev. B* **54**, 11169 (1996).
- [72] P. E. Blöchl, Projector augmented-wave method, *Phys. Rev. B* **50**, 17953 (1994).
- [73] J. P. Perdew, K. Burke, and M. Ernzerhof, Generalized gradient approximation made simple, *Phys. Rev. Lett.* **77**, 3865 (1996).
- [74] See Supplemental Material for details of comparison of band structure and DOS with experimental and theoretical lattice parameters, electronic structures at 14.1 GPa, comparison of DFT and Wannier band structure, orbital-projected band structure for each element at 90 GPa, main tight-binding parameters, introduction to SM-FRG, and summary of experimental  $T_c$  and calculated DOS under different pressures, and which includes Refs. [75-81].
- [75] P. Kopietz, L. Bartosch, and F. Schütz, Introduction to the Functional Renormalization Group (Springer, Berlin, 2010).
- [76] J. Berges, N. Tetradis, and C. Wetterich, Non-perturbative renormalization flow in quantum field theory and statistical physics, *Phys. Rep.* **363**, 223 (2002).
- [77] N. Dupuis, L. Canet, A. Eichhorn, W. Metzner, J. M. Pawłowski, M. Tissier, and N. Wschebor, The nonperturbative functional renormalization group and its applications, *Phys. Rep.* **910**, 1 (2021).
- [78] W.-S. Wang, Y.-Y. Xiang, Q.-H. Wang, F. Wang, F. Yang, and D.-H. Lee, Functional renormalization group and variational Monte Carlo studies of the electronic instabilities in graphene near 1/4 doping, *Phys. Rev. B* **85**, 035414 (2012).
- [79] Y.-Y. Xiang, F. Wang, D. Wang, Q.-H. Wang, and D.-H. Lee, High-temperature superconductivity at the FeSe/SrTiO<sub>3</sub> interface, *Phys. Rev. B* **86**, 134508 (2012).
- [80] W.-S. Wang, Z.-Z. Li, Y.-Y. Xiang, and Q.-H. Wang, Competing electronic orders on kagome lattices at van

- Hove filling, [Phys. Rev. B \*\*87\*\*, 115135 \(2013\)](#).
- [81] W. Metzner, M. Salmhofer, C. Honerkamp, V. Meden, and K. Schönhammer, Functional renormalization group approach to correlated fermion systems, [Rev. Mod. Phys. \*\*84\*\*, 299 \(2012\)](#).
- [82] N. Marzari and D. Vanderbilt, Maximally localized generalized Wannier functions for composite energy bands, [Phys. Rev. B \*\*56\*\*, 12847 \(1997\)](#).
- [83] I. Souza, N. Marzari, and D. Vanderbilt, Maximally localized Wannier functions for entangled energy bands, [Phys. Rev. B \*\*65\*\*, 035109 \(2001\)](#).
- [84] G. Pizzi, V. Vitale, R. Arita, S. Blügel, F. Freimuth, G. Géranton, M. Gibertini, D. Gresch, C. Johnson, T. Koretsune, J. Ibañez-Azpiroz, H. Lee, J.-M. Lihm, D. Marchand, A. Marrazzo, Y. Mokrousov, J. I. Mustafa, Y. Nohara, Y. Nomura, L. Paulatto, S. Poncé, T. Ponweiser, J. Qiao, F. Thöle, S. S. Tsirkin, M. Wierzbowska, N. Marzari, D. Vanderbilt, I. Souza, A. A. Mostofi, and J. R. Yates, Wannier90 as a community code: new features and applications, [J. Phys.: Condens. Matter \*\*32\*\*, 165902 \(2020\)](#).
- [85] Q.-K. Tang, L. Yang, D. Wang, F.-C. Zhang, and Q.-H. Wang, Spin-triplet  $f$ -wave pairing in twisted bilayer graphene near 1/4-filling, [Phys. Rev. B \*\*99\*\*, 094521 \(2019\)](#).
- [86] Q.-G. Yang, K.-Y. Jiang, D. Wang, H.-Y. Lu, and Q.-H. Wang, Effective model and  $s_{\pm}$ -wave superconductivity in trilayer nickelate  $\text{La}_4\text{Ni}_3\text{O}_{10}$ , [Phys. Rev. B \*\*109\*\*, L220506 \(2024\)](#).